arXiv:astro-ph/0109089v2 16 Dec 2001

Supernovae in Deep Hubble Space Telescope Galaxy Cluster Fields: Cluster Rates and Field Counts[1]

Avishay Gal-Yam[2,3], Dan Maoz[2,4], and Keren Sharon[2]
[1] *Based on observations made with the Hubble Space Telescope, which is operated by AURA, Inc., under NASA contract NAS5-26555.*
[2] *School of Physics & Astronomy and Wise Observatory, Tel Aviv University, Tel Aviv 69978, Israel; avishay@wise.tau.ac.il*
[3] *Colton Fellow.*
[4] *Department of Astronomy, Columbia University, 550 W. 120th St., New York, NY 10027, USA; dani@wise.tau.ac.il*

Accepted - . Received - ;

ABSTRACT

We have searched for high-redshift supernova (SN) candidates in multiple deep Hubble Space Telescope (*HST*) archival images of nine galaxy-cluster fields. We detect six apparent SNe, with $21.6 \leq I_{814} \leq 28.4$ mag. There is roughly 1 SN per deep ($I_{814} > 26$ mag), doubly-imaged, WFPC2 cluster field. Two SNe are associated with cluster galaxies (at redshifts $z = 0.18$ and $z = 0.83$), three are probably in galaxies not in the clusters (at $z = 0.49$, $z = 0.60$, and $z = 0.98$), and one is at unknown z. After accounting for observational efficiencies and uncertainties (statistical and systematic) we derive the rate of type-Ia SNe within the projected central $500h_{50}^{-1}$ kpc of rich clusters: $R = 0.20^{+0.84}_{-0.19}h_{50}^2$ SNu in $0.18 \leq z \leq 0.37$ clusters, and $R = 0.41^{+1.23}_{-0.39}h_{50}^2$ SNu in clusters at $0.83 \leq z \leq 1.27$ (95 per cent confidence interval; 1 SNu $\equiv$ 1 SN century^{-1} per $10^{10}L_{B\odot}$). Combining the two redshift bins, the mean rate is $R_{\bar{z}=0.41} = 0.30^{+0.58}_{-0.28}h_{50}^2$ SNu. The upper bounds argue against SNe-Ia being the dominant source of the large iron mass observed in the intra-cluster medium. We also compare our observed counts of field SNe (i.e., non-cluster SNe of all types) to recent model predictions. The observed field count is $N \leq 1$ SN with $I_{814} \leq 26$ mag, and $1 \leq N \leq 3$ SNe with $I_{814} \leq 27$ mag. These counts are about two times lower than some of the predictions. Since the counts at these magnitudes are likely dominated by type-II SNe, our observations may suggest obscuration of distant SNe-II, or a SN-II luminosity distribution devoid of a large high-luminosity tail.

Key words: galaxies: clusters: general – supernovae: general.

1 INTRODUCTION

The search for distant supernovae (SNe) has been revolutionised in the last few years by two cosmology-oriented groups, the Supernova Cosmology Project (SCP; Perlmutter et al. 1997), and the High$-z$ SN Search Team (Schmidt et al. 1998). Both groups have discovered hundreds of distant SNe with redshifts up to $z = 1$, and beyond. Analysis of these data shows evidence for an accelerating Universe, possibly driven by a positive cosmological constant (Riess et al. 1998; Perlmutter et al. 1999). Two likely high$-z$ SNe have also been discovered in a repeated observation with the Hubble Space Telescope (*HST*) of the Hubble Deep Field (HDF; Gilliland, Nugent, & Phillips 1999). One of these SNe has been shown by Riess et al. (2001) to be a type-Ia at $z = 1.7$, at an epoch before the transition from deceleration to acceleration. A third possible SN candidate was detected in the original HDF data through the analysis of the time dependent flux variation of objects in this field (Mannucci & Ferrara 1999). These observations demonstrate that deep *HST* observations are an efficient way to find high$-z$ SNe, with the high angular resolution and low sky background compensating for the small field of view.

Apart from the use of type-Ia SNe as standard candles, it is important to find and characterise distant SNe of all types. SN rates as a function of redshift probe the star formation history of the Universe, the physical mechanisms leading to SN-Ia explosions, and the cosmological parameters (Jorgensen et al. 1997; Sadat et al. 1998; Ruiz-Lapuente & Canal 1998; Madau, Della Valle, & Panagia 1998; Yungelson & Livio 2000). Furthermore, even in the absence of redshift information, SN number counts as a function of limiting magnitude can provide valuable constraints (Dahlén & Fransson 1999, hereafter DF; Sullivan et al. 2000, hereafter S2000).

© 0000 RAS

There are incentives to search for high$-z$ SNe not only in "blank" fields, but also in the fields of rich galaxy clusters. The lensing magnification of background sources by the cluster potentials enables detection of distant and intrinsically dim sources, that would be too faint to study otherwise. Indeed, the natural telescopes provided by rich clusters have been used successfully for deep studies of high$-z$ galaxies in the X-ray (Crawford et al. 2001), optical (e.g., Frye & Broadhurst 1998, Pettini et al. 2000), IR (e.g., Lemonon et al. 1998), and submm (Smail et al. 1998) regimes. Following the same reasoning, S2000 have considered the prospects of searching for high$-z$ SNe lensed by galaxy clusters. The most distant SNe could be found, with implications both for the cosmological applications and for our understanding of the nature of SNe.

Lensed high$-z$ SNe behind galaxy clusters could also probe the properties of the cluster lenses. For instance, a magnified type-Ia SN would provide a direct measurement of the cluster magnification, lifting the so called "mass-sheet degeneracy" encountered when deducing cluster masses from weak-lensing shear maps (Kolatt & Bartelmann 1998). A SN in a host galaxy that is lensed by a cluster into a giant arc may be multiply imaged into three images with time delays of weeks to months (Kovner & Paczynski 1988). SNe in galaxies that are nearly lensed into optical Einstein rings, such as the CL0024+16 arc system (Tyson, Kochanski, & dell'Antonio 1998), may also have short time lags (months to years) between images of the SNe in distinct galaxy images, providing constraints on the cluster mass distribution and on cosmological parameters.

Finally, knowledge of the rate of SNe *in* the galaxy clusters, as a function of SN type and cluster redshift, could illuminate several puzzles concerning the intra-cluster medium (ICM). One such puzzle is the total observed mass of iron, which is at least several times larger than that expected from SNe, based on the present-day stellar masses, and assuming a standard stellar initial mass function (IMF; e.g., Brighenti and Mathews 1998; Loewenstein 2000). Another is the energy budget of the ICM gas and the "entropy floor" observed in clusters, which suggest a non-gravitational energy source to the ICM, again several times larger than the expected energy input from SNe (e.g., Lloyd-Davies, Ponman, & Cannon 2000; Tozzi & Norman 2001; Brighenti & Mathews 2001). Proposed solutions to these problems have included an IMF skewed toward high-mass stars (so that a large number of iron-enriching core-collapse SNe are produced per present-day unit stellar luminosity), or a dominant role for SNe-Ia in the ICM enrichment. The latter option would require early-type galaxies in clusters to have SN-Ia rates much higher than observed in nearby field ellipticals. Constraints on these scenarios can be obtained by directly measuring the SN rate in clusters at various redshifts.

Observationally, SN searches in galaxy clusters were pioneered in the late 1980's by Norgaard-Nielsen et al. (1989), resulting in the first detection of a $z = 0.31$ SN in the galaxy cluster AC118. More recently, low-redshift cluster samples have been monitored for SNe by the Mount Stromlo Abell Cluster SN Search (Reiss et al. 1998) and by the Wise Observatory Optical Transients Search (Gal-Yam & Maoz 1999, 2001). To extend these efforts to higher$-z$ clusters, we have carried out a search for SNe in duplicate deep cluster images in the *HST* archive. In this paper, we describe our discovery of six SNe in this data set. We then use these SNe to derive the SN-Ia rate in clusters and to test the theoretical predictions for the non-cluster SN number counts in such fields. Where applicable, we assume a flat cosmology with parameters $\Omega_m = 0.3$ and $\Omega_\Lambda = 0.7$, and use h_{50} to denote the Hubble parameter in units of 50 km s^{-1} Mpc^{-1}.

2 ARCHIVAL TARGET SELECTION AND ANALYSIS

We have searched the *HST* archive for duplicate WFPC2 observations of galaxy cluster fields. Clusters were identified as such by the target name, or, when the names were not revealing, by searching the NED database for known clusters near the field coordinates. The details of our final cluster sample are given in Table 1. For two WFPC2 observations to be considered duplicates, we required that they had been obtained through the same filter, and that the angular distance between their field centres was less than 75 arcsec. The requirement for identical filters is due to the need for accurate image subtraction when searching for faint transients. The angular separation criterion is driven by the peculiar shape of the WFPC2 field, coupled with the random *HST* orientations, which can result in observations that are nominally duplicate, but have little overlap area.

To optimise the search for SNe, especially at high z, where cosmological time-dilation is important, we required a minimal time separation between data sets of 30 days. The implications of this criterion are accounted for in the analysis of our results. Finally, we have limited our search to deep observations, with total exposure times of at least 2000 s in one of the broad-band *HST* filters. In order to facilitate reasonable rejection of cosmic rays and hot pixels, we required that at least one of the duplicate data sets consist of at least three sub-exposures. When both duplicate data sets had three or more sub-exposures, we searched for candidate variable objects in both. In cases where only one of the data sets was suitably split, the other set was used only as a reference, since the possibility of cosmic ray events mimicking transient objects could not be ruled out. We have found nine galaxy cluster fields with observations in the *HST* archive satisfying these criteria. The overlap between images from different epochs is partial, so the total effective area useful for a bi-directional search is 30.8 arcmin^2, or 6.6 times the total area of WFPC2, excluding the PC1 CCD (see Table 1).

Sets of WFPC2 images at a given epoch were combined using software based mainly on the *DITHER* package (Fruchter & Hook, 1997) within IRAF *. A flexible, high-fidelity algorithm was used to reject cosmic-rays and hot/cold pixels, even in stacks with as few as three sub-exposures, allowing their use in this project. The PC1-CCD data were not used in the analysis, due to the lower sensitivity, the relatively small addition of area, and the need

---

* IRAF (Image Reduction and Analysis Facility) is distributed by the National Optical Astronomy Observatories, which are operated by AURA, Inc., under cooperative agreement with the National Science Foundation.

Table 1. Galaxy Cluster Fields with Duplicate *HST* Observations

Cluster	z	Epoch (UT Start)	Exposure [ks]	Sub-frames	Filter	Program ID	Overlap Area[a] [arcmin^2]	Number of Apparent SNe
Abell 2218	0.18	Mar 11 1999	8.4	12	F606W	7349	4.69	1
		Jan 13 2000	10.0	10	F606W	8500	4.69	-
Abell 1689	0.18	Jun 27 1996	2.0	2	F814W	6004	0	-
		Jun 19 1997	4.0	4	F814W	6004	4.69	-
		Jul 07 1997	4.6	4	F814W	5993	1.56	-
		Feb 24 2000	4.0	4	F814W	8546	1.56	-
AC114	0.31	Jan 06 1996	16.6	6	F702W	5935	1.28	-
		Oct 26 1997	15.6	6	F702W	7201	1.28	-
MS1512.4+3647	0.37	Mar 19 1996	6.3	9	F555W	6003	2.30	-
		Jun 20 1997	10.4	8	F555W	6832	2.30	-
MS2053.7−0449	0.58	Oct 23 1995	2.6	2	F814W	5991	0	-
		Sep 25 1998	3.2	3	F814W	6745	4.42	-
MS1054.4−0321	0.83	Mar 13 1996	15.6	6	F814W	5987	4.69	3
		May 29 1998	6.6	6	F814W	7372	4.69	-
CL1604+4304	0.89	Feb 25 1994	32.0	16	F814W	5234	3.97	1
		Feb 28 1995	32.0	16	F814W	5234	3.97	1
RXJ0848.6+4453	1.27	Mar 01 1999	13.9	5	F814W	6812	4.69	-
		Apr 15 1999	13.9	5	F814W	6812	4.69	-
CL1645+46	> 2.8	May 7 1997	6.0	12	F814W	6598	3.42	-
		Sep 30 1999	5.3	4	F814W	7342	3.42	-

Notes:
[a] The overlap area is set to zero for data sets with fewer then three sub-exposures. These data sets are used only as references for searching for SNe at other epochs (§ 3.3.3).

to resample the data in order to compare to WF-CCD data from other epochs.

The combined images of a cluster from two available epochs were registered, using a general geometrical transformation, calculated from the positions of ~ 20 compact galaxies or stars, visible at both epochs. The images were scaled according to their exposure times and subtracted, forming a difference image. The stable *HST* point-spread function (PSF) allows for good cancellation of almost all non-variable objects, as shown in an example in Fig. 1. Some low-level residuals remain in the difference images near bright stars and at the nuclei of the brightest galaxies. These residuals are unlikely to mimic real objects, since their suspect origin is evident from the images. However, the residuals near galactic nuclei limit the detection of nuclear variability in these galaxies, either SNe close to the nucleus or active galactic nuclei (AGN). This is taken into account by our detection efficiency simulations, described in § 3.3.2.

The difference images were methodically scanned by eye, and all residual objects checked and classified. After the elimination of obvious subtraction artefacts, the location of each residual object was checked in each of the sub-exposures from that epoch. For a candidate to be considered secure, we required that it have a stellar PSF, and appear in at least three independent subsets of the data, each consisting of the sum of individual exposures in which its location is not obviously affected by cosmic rays, with non-variable flux levels, to within errors. This criterion eliminates residual events consisting of cosmic rays that are coincident in several sub-exposures, as well as chip defects and rare, high amplitude, background fluctuations, since in these cases most of the candidate's flux in the final combined image comes from only some of the available sub-exposures.

Care was taken not to reject real events affected by cosmic ray hits, even in data sets with few sub-exposures. Real events could, in principle, be lost in three-image data sets if cosmic rays happened to hit the object's location on two of the three sub-exposures. However, given that only 1-2 per cent of the pixels in each image are affected by cosmic rays, this has a probability of $\sim 10^{-4}$, and much lower in data sets with more than three sub-exposures. Candidates that passed these criteria were considered real transient or variable sources, most likely high$-z$ SNe (see §3.2). In practice, all but one of the transient sources we found can be identified on each individual exposure, and not only in summed subsets. Figure 2 shows an example.

The flux limit at each epoch depends on the length of the exposures and the filter used, and therefore varies between our sample clusters, but in all sets the limit for > 50 per cent detection is better than $I_{814} = 26$ mag†.

3 RESULTS

3.1 Apparent supernovae

We have detected six apparent SNe in the cluster fields we have searched, including the rediscovery of SN 1996cl, which was previously known. For each SN, Table 2 lists the details, and Fig. 3 shows a section of the images at two epochs. Among the six SNe, five are projected within 2.5 half-light

---

† We report our observations using the AB magnitude system, in which the magnitude in a band b centered at wavelength λ [nm] is $b_\lambda = -48.6 - 2.5 \times \log f_\nu$, where f_ν is the flux density at frequency ν in erg s^{-1} cm^{-2} Hz^{-1}.

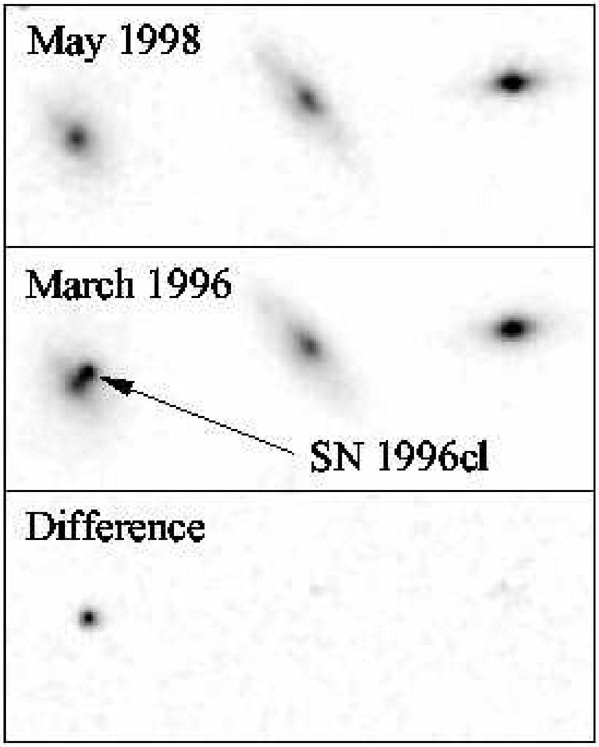

Figure 1. Example of image subtraction; SN 1996cl, in a galaxy in cluster MS1054.4−0321, in a $8\farcs5 \times 3\farcs6$ section of the difference image (lower panel) created by subtracting the data obtained in May 1998 (upper panel) from the data of the same field taken during March 1996 (middle panel). Note the clean subtraction of the galaxies, resulting from the stable *HST* point-spread function.

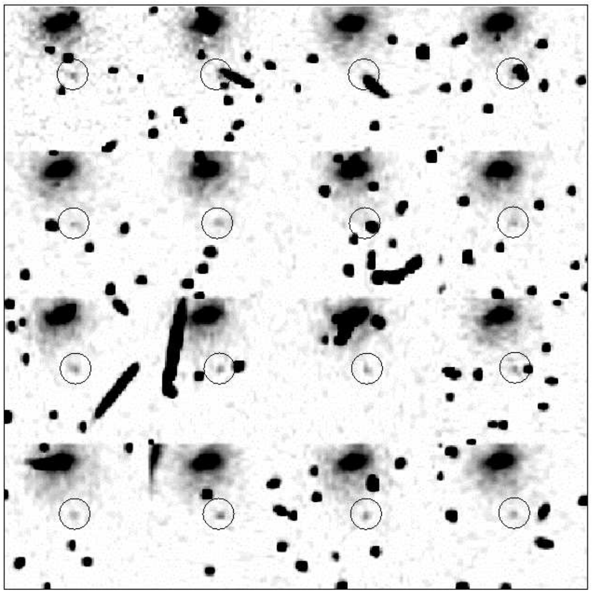

Figure 2. Example of candidate verification; $2\farcs1 \times 2\farcs1$ sections of the individual WFPC2 exposures at the location of SN 1995bf in CL1604+4304. The apparent SN is visible in all sub-exposures where the location is not affected by cosmic-ray hits, with a stellar PSF and constant flux, to within the expected errors.

radii of galaxies that are likely their hosts, while the sixth has no obvious host (but see § 3.1.2). We have been able to determine the redshift and types of the host galaxies of five events from the literature (see below). As noted in proof by S2000, the object they previously considered a SN candidate, near the core of AC114, is not variable. Indeed, Campusano et al. (2001) show that this object is likely one of the images of a multiply-lensed background galaxy (marked A4 in their Fig. 1). We briefly discuss each SN below.

3.1.1 SN 1999gv in the field of Abell 2218

During March 1999, a large mosaic (22 positions) of WFPC2 images, covering the entire field of Abell 2218, was obtained through the F606W filter. The main goal of this program (PI Squires) was to create weak lensing shear maps, and to compare the resulting mass distribution to that derived via strong lensing, X-rays, and the Sunyaev–Zeldovich effect. In January 2000, following the Space Shuttle servicing mission 3a, the cluster was re-imaged through the F450W, F606W, and F814W filters as an "early release" observation, intended to demonstrate the telescope performance. Comparison between the 8.4-ks F606W image from March 1999 and the 10.0-ks F606W image from January 2000, reveals a bright unresolved object in the 1999 exposure (Gal-Yam & Maoz 2000; see Fig. 3). The host galaxy is catalogued as No. 149 in Le Borgne et al. (1992), where it is classified as an elliptical galaxy with $B = 19.9$ mag and redshift $z = 0.1753$. In view of the brightness of this SN, and its association with an elliptical cluster member, it is most likely a type-Ia SN in the cluster. Assuming a typical SN-Ia, the apparent magnitude suggests a SN age of ~ 25 days past maximum light.

3.1.2 SNe 1996cl, 1996cp, and 1996cq in the field of MS1054.4−0321

The core of the distant galaxy cluster MS1054.4−0321 ($z = 0.83$) was observed with the F814W filter during March 1996, in a program to study distant, X-ray selected clusters (PI Donahue). It was re-observed in May 1998, as part of a shallower, wide field mosaic (PI Franx), designed for a morphological large-scale study. A comparison of the images from the two epochs reveals three apparent SNe (Gal-Yam, Sharon, & Maoz 2001).

The brightest of the three is SN 1996cl, originally discovered by the SCP in ground-based data obtained on March 18, 1996 (Perlmutter et al. 1996), and spectroscopically confirmed as a type-Ia SN at the cluster redshift. In the *HST* observation, obtained 5 days prior to that of Perlmutter et al., the SN is detected with $I_{814} = 23.71$ mag, the magnitude expected for SN-Ia some 10 days (~ 5.5 days in the SN rest frame) before peak magnitude.

A second transient object in this field, SN 1996cq, is detected at $I_{814} = 25.61$ mag, without any obvious host galaxy. This object is superposed on a faint fuzz near the image detection limit that may be a low-surface-brightness galaxy associated with it.

The third transient source is SN 1996cp, with $I_{814} = 26.7$ mag. This object is superposed on a small knot of emis-

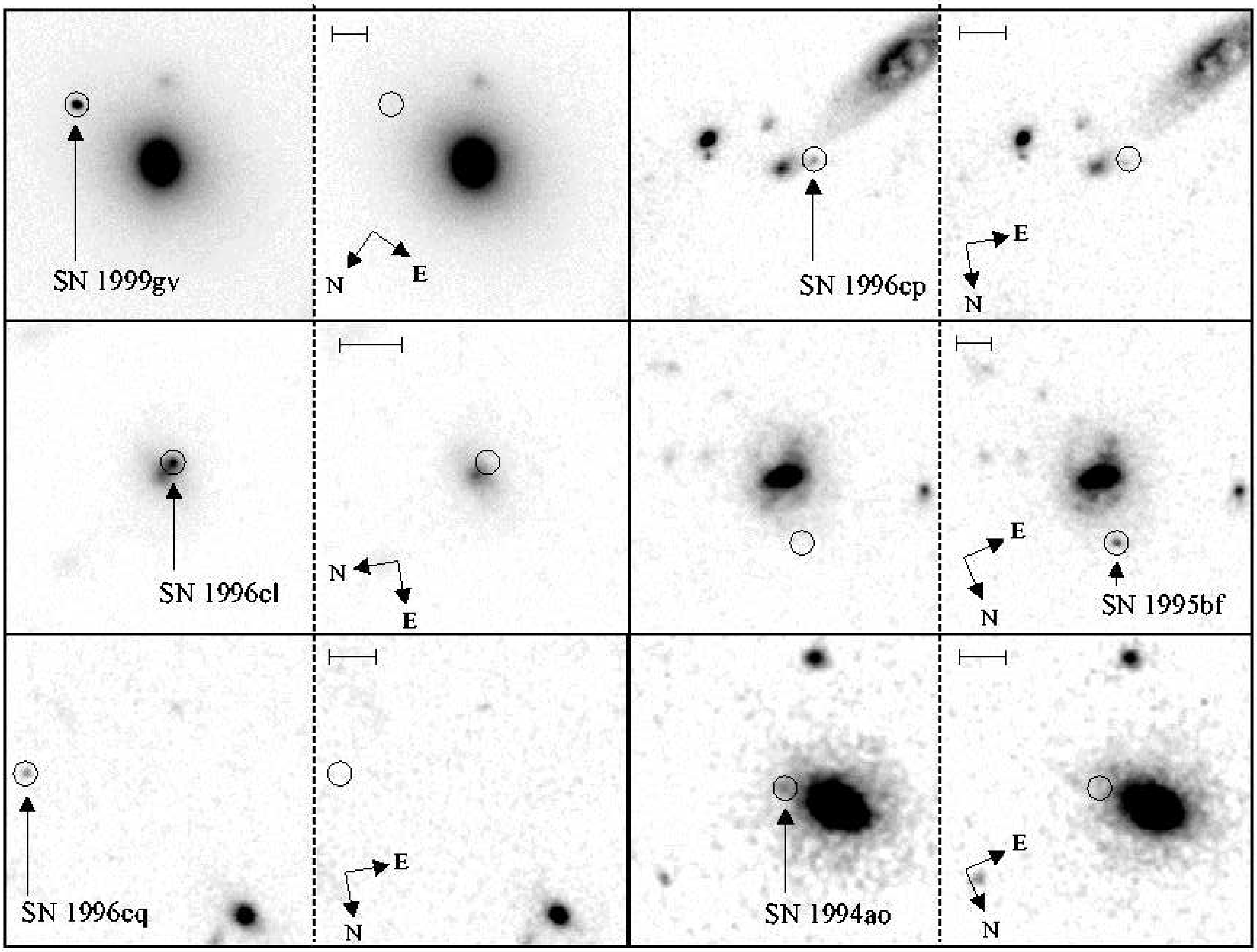

Figure 3. Sections of the images, at two epochs, for each of the six apparent SNe. The scales shown in the upper-left-hand corners correspond to 1″.

Table 2. Apparent Supernovae

SN	Cluster Field	Magnitude	α (2000)	δ (2000)	Offset from Host	Host z
1999gv	Abell 2218	$V_{606} = 21.64 \pm 0.03$	$16^h36^m02.2^s$	+66°12′34”	0.″8 S 2.″8 W	0.175
1996cl	MS1054.4−0321	$I_{814} = 23.71 \pm 0.04$	$10^h56^m59.1^s$	−3°37′36”	0.″1 S 0.″05 W	0.827
1996cq	MS1054.4−0321	$I_{814} = 25.61 \pm 0.05$	$10^h57^m02.2^s$	−3°37′34”	-	?
1996cp	MS1054.4−0321	$I_{814} = 26.7 \pm 0.2$	$10^h57^m03.5^s$	−3°37′41”	0.″9 E	0.596[a]
1995bf	CL1604+4304	$I_{814} = 26.14 \pm 0.06$	$16^h04^m20.4^s$	+43°04′44”	2.″9 N 0.″6 W	0.985
1994ao	CL1604+4304	$I_{814} = 28.4 \pm 0.5$	$16^h04^m23.3^s$	+43°03′56”	1.″4 S 1.″1 W	0.496

Notes:
[a] Other host galaxies possible, see text.

sion, 0.9 arcsec due east from the nucleus of a blue, late type galaxy with $z = 0.60$ (Milvang-Jensen et al. 2002). However, it could also be associated with a larger spiral galaxy that is found 4.1 arcsec to the south-east, catalogued as No. 1403 by van Dokkum et al. (2000), who classify it as a cluster member with $z = 0.81$. Since the emission knot which hosts SN 1996cp is closer to the $z = 0.60$ galaxy and has similar $I_{814} - V_{606}$ colours, we adopt a redshift of $z = 0.60$ for this SN. However, we cannot at this time exclude the possibility that the SN is associated with the nearby cluster galaxy (No. 1403) or that the emission knot is a separate galaxy altogether. Derivation of photometric redshifts for the emission knot hosting SN 1996cp from multi-color images of this cluster may shed more light on this issue.

3.1.3 *SNe 1994ao and 1995bf in the field of CL1604+4304*

The cluster CL1604+4304 ($z = 0.89$) was the target of a deep observation in 1994 (32 ks through the F814W filter; PI Westphal). However, a pointing error placed the target ~ 20 arcsec from the designated position. The cluster was therefore re-imaged one year later, again for 32 ks. Subtraction of these two deep images reveals two SNe (Gal-Yam et al. 2001). The first, SN 1995bf, with $I_{814} = 26.14$ mag, is found near a putative host, catalogued by Lubin et al. (1998) as No. 019, an Sb galaxy with $z = 0.985$, i.e., behind the cluster.

The limiting magnitude for SN detection in these particular images, derived from our detection-efficiency simulations (see §3.3.2), is $I_{814} = 29$ mag, if the requirement that the SN appear in individual sets of sub-exposures is relaxed, to the effect that candidates need be detected with a stellar PSF and constant flux in only two independent subsets of the data. This analysis reveals a second, very faint, apparent SN in this cluster. SN 1994ao has $I_{814} = 28.4$ mag, near the detection limit, and is the faintest SN detected to date (~ 1.5 mag fainter than SN 1997ff; Gilliland et al. 1999; Riess et al. 2001). This object is near an S0 galaxy with $z = 0.496$, in the cluster foreground (No. 028 of Lubin et al. 1998). If the event is indeed associated with this host, it could imply it is a SN Ia, as core-collapse SNe (types II, Ib, Ic) are generally not found in S0 galaxies. However, the absence of core-collapse SNe in S0 galaxies has only been established in low redshift ($z \leq 0.1$) environments. If this is indeed a type-Ia SN, then the low luminosity implies it is many months past maximum. We report this event as an example of the capability of *HST* to find very faint SNe, but do not include it in our quantitative analysis of the results, below.

3.2 Supernova alternatives

Apart from SN 1996cl, all the apparent SNe we discuss lack spectroscopic confirmation. We now consider alternative explanations, other than SNe, for the observed objects, and argue that all are unlikely.

Solar system objects – Small bodies in the Solar System (e.g., Kuiper Belt objects – KBOs; Trujillo, Jewitt & Luu 2001, and references therein) can potentially mimic transients. To pose as one of our apparent SNe, such an object must be faint ($I_{814} > 22$ mag) and slowly moving. However, the combination of relatively long observing periods (hours to days) with the *HST* resolution allows us to set firm upper limits on the proper motions of the detected transient events. For the relevant data set with the shortest observing period (MS1054.4−0321), the upper limit on the motion of the transients is $\mu \leq 0.12''\mathrm{day}^{-1}$. For all three fields in which we have found SN candidates, the expected parallaxes of a KBO at 50 AU, in the field directions and at the times of observation, as a result of the Earth's orbital motion, are $> 70''\mathrm{day}^{-1}$. This is much larger than our upper limit. We note that the proper motion of a KBO at several tens of AU from the Sun cannot be large enough to offset the effect of the Earth's parallax, so that KBOs, regardless of their exact orbital parameters, cannot account for any of the events we discuss.

Variable Galactic stars – The fainter ($I_{814} \sim 26$ mag) among the transient events we have discovered are generally too faint to be plausible variable Galactic objects. Such objects would need to vary by at least ~ 1 mag in order to fall below the detection limit on one of the epochs. A chromospherically active $I = 27$ mag M4 dwarf (which, say, flared into our detection range), would be at a distance of 40 kpc, far out in the low-stellar-density halo, and hence highly unlikely to turn up in such a small field. Cataclysmic variables in quiescence will always be brighter at minimum light than a single M-dwarf. Our only SN candidate brighter than $I_{814} = 25.5$ that lacks spectroscopic confirmation, SN 1999gv in Abell 2218, could be a bright flare from a Galactic G- or K-dwarf. However, the lack of any evidence for such flares at this position in numerous previous images of Abell 2218, obtained over several years through various telescopes (e.g., Gal-Yam & Maoz 2000), makes this possibility unlikely.

Variable stars in other galaxies – If the transient events we have found are associated with the galaxies near to which they are projected, then they are generally too luminous to be anything but SNe. Of the six events we discuss, the redshifts of the probable hosts of five events are known (Table 2). The most luminous novae have absolute magnitudes $M_I = -11$ (Della Valle 1991; Warner 1995) and thus would be far too faint to be detected at the redshifts of these galaxies, falling below $I \sim 28.5$ mag at $z \sim 0.17$. The host galaxy of SN 1996cq is only marginally detected in the deep *HST* image. If this event is a nova, the implied luminosity of the host becomes implausibly low, $M_I > -8.7$ mag.

Active galactic nuclei – None of the events we discuss are located in the nuclei of the putative host galaxies, and hence are not Seyfert-like AGN. The candidates could, in principle, be more distant, highly variable quasars in the nuclei of undetected galaxies, projected by chance within < 2.5 half-light radii of the galaxies that are seen in five of six cases. By performing aperture photometry for all the galaxies in each image, we have determined the galaxies' half-light radii. We find that, even in the most crowded fields, < 5 per cent of the total area we have searched is within 2.5 half-light radii of a galaxy. For SN 1996cq, whose candidate host is barely detected, the quasar option cannot be ruled out as firmly.

Gamma-ray burst afterglows – Recent observations of gamma-ray burst optical afterglows suggest that these explosions are not isotropic (e.g., Frail et al. 2001, and references therein). If the gamma rays are more beamed than the optical emission, there may be many optical afterglows that have no corresponding gamma-ray burst (Rhoads 1997). Such events could, in principle, explain some of the transients we have discovered. However, recent work by Dalal, Griest, & Pruet (2001) shows that even a continuous monitoring campaign reaching a limiting magnitude of $R = 27$ is expected to yield < 0.15 events $\mathrm{deg}^{-2}\ \mathrm{yr}^{-1}$. Our search has visited a total area $< 0.01\ \mathrm{deg}^2$, only twice.

We conclude that most or all of the events we have discovered are likely bona-fide SNe. Nevertheless, in our derivation of cluster SN-Ia rates and field counts, the estimated uncertainties account for the more ambiguous identifications of several of the candidates. In our comparisons of field counts to some theoretical predictions (§3.3.3), if any of the events were not SNe, the discrepancy between observations and some models would only grow.

3.3 Field supernova counts

3.3.1 Observed counts

Of the six apparent SNe we have detected, three have $I_{814} \leq 26$ mag, five have $I_{814} \leq 27$ mag, and one has $I_{814} \sim 28.4$ mag. SN 1996cl in MS1054.4−0321 is a spectroscopically verified cluster event, and SN 1999gv in Abell 2218 is also most likely associated with a cluster galaxy. Thus, our upper limits on the detected field (i.e., non-cluster) SN counts, is one event with $I_{814} \leq 26$ and three events with $I_{814} \leq 27$. These observational results can be compared directly with theoretical predictions for the number of SNe expected in deep WFPC2 images.

The data in our sample were obtained with a variety of filters and exposure times. Converting our results to absolute number counts (i.e., SNe per unit sky area, visible at some moment to a given flux limit) is further complicated by a dependence on poorly known parameters for core-collapse SNe. Instead, we take the published theoretical predictions, fold them through our observational parameters, apply the model assumptions self-consistently, and derive the expected numbers of SNe in our particular sample. We then test the models by direct comparison of the expected numbers to the observations.

3.3.2 Detection efficiencies

We have carried out simulations in order to estimate our SN detection efficiencies. Several tens of artificial point sources ("fake" SNe) with known flux and the proper amount of Poisson noise were blindly added to the data for each field. The fake SNe were distributed such that the probability that a galaxy hosts a fake SN is proportional to the galaxy brightness. The separation of a SN from the galaxy centroid was chosen from a Gaussian distribution with σ equal to 0.85 times the galaxy's half-light radius. Thus, the fake-SN distribution follows the galactic light. Although in reality the SNe should follow the galactic *luminosity*, flux is a reasonable surrogate; the cluster galaxy population in a given field is all at a similar distance, and most of the field galaxies are likely also in a limited redshift range. Our procedure is also conservative, in the sense that it places the fake SNe on too-high galactic backgrounds, leading to an underestimate of the true efficiency, since cosmological surface-brightness dimming increases the contrast between a SN and its host-galaxy background at high redshifts. In principle, one might place some fake SNe at blank sky positions, to represent SNe in host galaxies that are below the detection limit. We find that our detection efficiency for such objects is significantly higher than for objects placed on galactic backgrounds. However, having no concrete estimate for the fraction of "hostless" SNe from the total population, and in line with our conservative approach, we did not include such events in the final simulations.

The simulated data were reduced and searched for SNe, like the real data, and the fraction of recovered objects noted. Examples of the efficiency curves for the shallowest (Abell 1689) and deepest (CL1604+4304) data sets are given in Table 3, and the relevant efficiency values for all fields are shown in Table 4.

Table 3. Sample Detection-Efficiency Values

Magnitude I_{814}	Efficiency Abell 1689	Efficiency CL1604+4304
23	0.95	1.0
24	0.90	1.0
25	0.80	1.0
26	0.45	0.85
27	0	0.60
28	0	0.50
29	0	0

Six of the nine clusters we discuss were observed through the F814W filter, which resembles the Kron–Cousins I filter. Model predictions for SN number counts in deep *HST* fields have been calculated for the I band (DF; S2000; see §3.3.3), and for these fields the comparison is straightforward. However, for three of the cluster fields, the duplicate observations were obtained through the F555W (Johnson V), F606W ("wide V"), and F702W ("wide R") filters.

A quantitative comparison of the observed V-band or R-band number counts with the expected I-band counts requires knowledge of the characteristic colours of the high−z SN population. While this information is fairly well known for type-Ia SNe (Perlmutter et al. 1999, Schmidt et al. 1998), beyond 25–26 mag, the counts are expected to be dominated by core-collapse SNe (e.g., DF; S2000). Broad-band photometry and spectroscopy of core-collapse SNe with $z > 0.5$, as well as UV spectra of local core-collapse SNe, for deriving K-corrections, are scarce (DF; Gilliland et al. 1999; S2000). As the colours of SNe depend strongly on the SN redshift, type, age, and extinction, the colour terms are highly model dependent. The relative fractions of the various sub-types of core-collapse SNe (II-P, II-L, IIn, Ib, and Ic) are observationally unknown at high-z, and must be assumed based on sparse data from local observations. With these limitation in mind, we pursue two alternative analyses.

First, following DF and S2000, we assume that the SN population probed by the data is dominated by type-II SNe at $z \sim 0.7$, about half of which are type II-P events. (The actual fraction of the various SN sub-types is controversial; we merely make the same assumptions as DF and S2000 in order to compare their models and our observations self-consistently.) Based on UV spectra of local type-II SNe, DF assume that type II-P SNe show a strong UV deficit as they enter the plateau phase, some 20 days after maximum light, while type-II-L and -IIn SNe do not have this effect. At high z, the type II-P SNe will therefore have red $V-I$ and $R-I$ colours. We estimate that about half of the type II-P SNe are observed close to maximum light, when $V-I$ and $R-I$ are close to zero (Fig. 10 of DF), and apply no colour correction to the efficiency for this fraction of the population. For the remaining type II-P SNe, observed at rest-frame ages $t \geq 20$ days, we adopt the colours calculated by DF, based on the SN models by Eastman et al. (1994). Converting the colours from Fig. 10 of DF to the magnitude system we use, we obtain $R_{702} - I_{814} = 0.75$ and $V_{555} - I_{814} \geq 2$. Since the

F606W filter extends further into the red than F555W, and has significantly higher sensitivity, we assume $V_{606} - I_{814} = 1.5$. The detection efficiency, η, that applies to the half of the type II-P SN population with ages $t \geq 20$ days (1/4 of the total SN population) is the efficiency found for the observed (non-I_{814}) band, at a magnitude obtained by adding the colour term. For example, in the Abell 2218 data set, the corrected efficiency at $I_{814} = 26.4$ mag is $[0.75 \times \eta(V_{606} = 26.4)] + [0.25 \times \eta(V_{606} = 26.4 + 1.5)] = [0.75 \times 0.63] + [0.25 \times 0] = 0.47$.

Alternatively, in order to compare our observed SN number counts with the predictions in the least model-dependent way, we consider only the sub-sample of six fields observed through the F814W filter, avoiding the problem of colour corrections altogether. This approach leads to slightly smaller number statistics, but the conclusions, presented below, remain unchanged.

In all but one of the data sets we have analyzed, the interval between epochs is ten months or longer, ample time for even the slowest SNe to vary significantly, even when time dilation at $z \sim 1$ is taken into account. The two epochs we compare in the case of RXJ0848.6+4453, however, are separated by only 44 days, equivalent to 22 rest-frame days for a $z = 1$ SN. Slowly-varying SNe IIn and SNe II-P during their plateau phase could become hard to detect in this data set. To correct for this possible bias, we again assume that about 1/2 of the high$-z$ SNe we expect to discover are SNe II-P. These are expected to be in the slowly varying phase of their light curve for about 1/3 of the time they are observable. We therefore estimate that 1/6 of the expected high$-z$ SNe would not be detected, and apply a correction of 5/6 to the core-collapse SN detection efficiency in this data set. One also needs to correct for the possibility that SNe observed on the rise in the first epoch would have approximately the same magnitude (within our observational error) when observed in the declining phase 44 days later, and thus avoid detection. Using simulated variable objects superposed on the actual images, we find that $I = 26$ objects can vary by at most 0.4 mag and still avoid detection. Applying this to typical light-curves for the various SN types, we estimate the about 15 per cent of the entire SN population might be lost. We therefore apply a further correction to our efficiency, with the final correction factor being $(5/6) \times 0.85 = 0.7$.

3.3.3 Comparison with theoretical predictions

S2000 have considered in detail the exact observational route we have taken – a search for SNe in deep, duplicate *HST* observations of galaxy cluster fields. Using models for the expected SN rates, and taking into account various models for the lensing effects of the clusters, S2000 have calculated the number of SNe expected when comparing two images of the same cluster from different epochs. They find that the SN number counts depend weakly on the lensing and star-formation models they use (Table 1 of S2000). The background SN number counts are weakly affected by lensing because the added depth given by the magnification is countered by the reduced effective area that is searched, due to that same magnification (Porciani & Madau 1999; S2000). We can therefore adopt representative values from S2000 for the number of SNe expected per WFPC2 field for a two-epoch visit. Converting the Vega-based magnitudes of S2000 (M. Sullivan, private communication) to AB magnitudes, their predicted counts are $N_p = 1.5$ SNe per WFPC2 field to $I_{814} \leq 26.4$ mag, and $N_p = 3$ SNe to $I_{814} \leq 27.4$ mag, in a bi-directional search (i.e., including SNe discovered in both epochs). Note that these numbers are for field SNe only, as S2000 exclude cluster events from their calculations. S2000 assume 5.71 arcmin^2 for the area of a WFPC2 field, while the correct value for the WF CCDs only is 4.69 arcmin^2, so we scale their predictions by 0.82.

In similar work, DF have also calculated the numbers and properties of high$-z$ SNe. Although they address mainly the expected number of SNe detectable with the Next Generation Space Telescope, in their Table 2 they also give the expected number of SNe in an *HST* WFPC2 field to $I_{800} = 27$ mag, equivalent to $I_{814} = 26.96$ mag. They predict a total of 0.5 SN per WFPC2 field per visit. We therefore adopt an expected number of $N_p = 1$ SN for every two-visit WFPC2 field reaching $I_{814} = 27$ mag. DF assume 5.0 arcmin^2 for the area of a WFPC2 field, while the value for the WF CCDs only is 4.69 arcmin^2, so we scale their prediction by 0.938.

In our calculations below, we will assume that 1/2 of the SNe with $I_{814} \leq 27$ mag have $I_{814} \leq 26$ mag, based on the results of S2000. We note that DF calculated the expected SN number counts in blank (non-cluster) fields, but because of the weak effect of cluster lensing on total background counts, these predictions can also be compared to our observations.

Given a predicted SN surface density on the sky, we can calculate the expected number of SNe in the observed sample. For each data set, we determine the effective area S useful for SN search. This is just the sum of the areas that overlap the area of a reference epoch. For example, if useful data sets are available for two epochs with complete overlap, the effective area is just twice the illuminated area of the WF chips, or 9.38 arcmin^2. In cases where one of the epochs cannot be searched, and was used only as a reference, its contribution to the effective area is zero. The predicted SN count per magnitude interval, dm, per observed cluster field is thus the surface density per magnitude interval, $n_p(m)dm$, times the fraction of a field effectively probed for SNe, times the search efficiency $\eta(m)$, with the latter modified by a colour term for data sets that were not observed in the I band (see §3.3.2):

$$n(m)dm = n_p(m) \times \frac{S}{9.38\mathrm{arcmin}^2} \times \eta(m)\ dm. \qquad (1)$$

The total SN counts expected per field to a given limiting magnitude can be obtained by integrating Eq. 1 over m. S2000 and DF list their results for the surface density of SNe, $N_p(< m)$, integrated up to some limiting magnitude, rather than the differential surface density $n_p(m)dm$. However, since the SN counts are a steeply rising function of magnitude, we can obtain a good approximation of the total by replacing the integral with the sum of two terms, for $I_{814} < 26.4$ (26) mag and for $26.4 \leq I_{814} \leq 27.4$ ($26 \leq I_{814} \leq 27$) mag, according to the cumulative numbers given by S2000 (DF), and weighted by $\eta(26.4)$ [$\eta(26)$] and $\eta(27.4)$ [$\eta(27)$], respectively. The effective areas, efficiencies, and predicted SN numbers for each cluster field are given in Table 4.

Summing over all fields, we obtain the total predicted

Table 4. Predicted Field SN Counts

Cluster	Effective area	Efficiency				Expected^c SN number (N)			
	(S)		(η)			S2000	S2000	DF	DF
	(arcmin^2)	$I = 26$	$I = 26.4$	$I = 27$	$I = 27.4$	$I \leq 26.4$	$I \leq 27.4$	$I \leq 26$	$I \leq 27$
Abell 2218	9.38	0.48^a	0.47^a	0.46^a	0	0.58	0.58	0.23	0.44
Abell 1689	7.81	0.45	0.29	0	0	0.30	0.30	0.18	0.18
AC 114	2.56	0.69^a	0.62^a	0.5^a	0.41^a	0.21	0.35	0.09	0.15
MS1512.4+3647	4.60	0.62^a	0.53^a	0.37^a	0	0.32	0.32	0.14	0.23
MS2053.7−0449	4.38	0.77	0.70	0	0	0.40	0.40	0.17	0.17
MS1054.4−0321	9.38	0.84	0.76	0.65	0	0.94	0.94	0.39	0.70
CL1604+4304	7.94	0.85	0.75	0.60	0.56	0.78	1.37	0.34	0.58
RXJ0848.6+4453	9.38	0.42^b	0.31^b	0	0	0.38	0.38	0.20	0.20
CL1645+46	6.84	0.82	0.72	0.51	0	0.65	0.65	0.28	0.45

Notes:
[a] Corrected with color term to convert to effective I-band efficiency (§3.3.2).
[b] Corrected to account for loss of slowly-fading SNe in data with short time interval between epochs (§3.3.2). There are no offsets between sub-frames of this data set, making the verification of faint ($I_{814} < 26.5$) point sources impossible. The efficiency for ($I_{814} > 26.5$) is therefore set to zero.
[c] The predictions of S2000 and DF, as given here, assume different cosmologies. For inter-comparison, the predictions of S2000 should be scaled down by a factor of 0.7 (see text).

SN numbers in the sample according to the models of S2000 and DF. These predictions are compared with our observations in Table 5.

Looking at Table 5, one sees that the counts predicted by both DF and S2000 are formally consistent with the observations. We note, however, that the predictions of S2000 are always higher than the observed values. Moreover, the observed numbers given in Table 5 are upper limits, since, however unlikely, some of the apparent SNe we discuss may not be SNe (§ 3.2). Also, the "non-cluster" SN sample includes objects (SNe 1996cp and 1996cq) for which the redshift is uncertain, and hence may actually be cluster events. Finally, (§ 3.3.2) our adopted efficiency values are likely underestimates, leading to too-low predictions. For instance, if SN 1996cp is, in fact, a cluster event (§ 3.1.2), the difference between the prediction of S2000 and the data becomes statistically significant.

It is therefore instructive to investigate the sources of the differences between the predictions of S2000 and DF. The two groups assume very similar star-formation histories for the Universe (e.g., compare Figure 1 of DF with Figure 2 of S2000). Each group assumes somewhat different forms for the delay functions of SNe-Ia (i.e., the SN-Ia rate as a function of time after an initial burst of star formation), but at these magnitudes, Ia's are a small fraction, 15–25 per cent, of all SNe, so this has little effect on the total counts. For the UV spectrum of type-II-P SNe during their plateau phase, DF use a truncated blackbody model, while S2000 use an empirical spectrum, but their details are very similar, and in any case, this is of little consequence, since at $I < 27$ mag the median redshift of the SNe is $z \sim 0.7$, where the I band probes rest-frame ~ 4800 Å. The $\Omega_m = 0.3$, $\Omega_\Lambda = 0.7$ cosmology assumed by S2000 leads only to a ~ 30 per cent increase in the total SN number to $I < 27$ mag, over that obtained using DF's assumed $\Omega_m = 1$ cosmology (P. Nugent, private communication).

The bulk of the discrepancy between the predictions of S2000 and DF stems from two subtle differences in the treatment of type-II SNe, for which S2000 predict ~ 2 times more counts than DF. First, S2000 use a larger value for the dispersion of peak absolute magnitudes of type II-L SNe ($\sigma = 1.3$ mag), derived from the full sample of local type II-L SNe discussed by Miller & Branch (1990), and including the "overluminous" II-L SNe 1979C and 1980K. DF use a smaller dispersion ($\sigma = 0.5$) derived from a sub-sample excluding the two overluminous SNe, but retain the (brighter) peak luminosity derived from the full II-L SN sample. The large dispersion chosen by S2000 results in a high-luminosity tail of type II-L SNe, a large number of which will be visible in a flux-limited SN search. Second, S2000 adopted a constant dust extinction value for all type-II SNe, of $A_V = 0.45$ mag, equivalent to $A_B = 0.66$ mag. DF used a minimum extinction value of $A_B = 0.32$ mag, lower than the one used by S2000, but modified it according to a random orientation of the host galaxy. This produced a large extinction for nearly edge-on hosts, with as many as 40 per cent of the core-collapse SNe suffering extinctions that are greater than 1 mag (T. Dahlén, private communication). This again, makes DF's SNe fainter than those of S2000, and the total predicted numbers lower.

Returning to our observational results, it appears that the combined assumptions of DF for the type-II SN peak magnitudes, dispersions, and dust extinctions may be a better description of the high$-z$ SN population than those used by S2000. Of course, other variations on these assumptions can be devised, which will produce the same predicted counts. Furthermore, some of the assumptions that are common to the models of both DF and S2000 could also be wrong, but counterbalanced by wrong SN-II parameters. With improved knowledge of the relative fraction of different SN types, their luminosity functions, and their spectra, the observed SN counts will be able to constrain some of the other parameters, such as the extinction of core-collapse SNe at high redshift.

Table 5. Observed vs. Predicted Field SN Counts

I_{814} mag	Observed (total) all bands	I_{814}	Observed (non-cluster) all bands	I_{814}	Expected (S2000) all bands	I_{814}	Expected (DF) all bands	I_{814}
≤ 26.4	4	3	2	2	4.56	3.45	-	-
≤ 27.4	5	4	3	3	5.28	4.03	-	-
≤ 26	3	2	1	1	-	-	2.01	1.55
≤ 27	5	4	3	3	-	-	3.09	2.27

3.4 Cluster supernova-Ia rates

3.4.1 Observed clusters and cluster supernovae

In this section, we deal with the type-Ia SNe in the clusters themselves. As opposed to the preceding discussion of the field SN counts, which are dominated by type-II's, the properties of SNe-Ia are homogeneous and well characterised. As a result, we can translate the observed numbers into absolute SN-Ia rates in rich clusters. We separate the clusters into two subsamples, a low-z sample consisting of four clusters at $0.18 \leq z \leq 0.37$, and a high-z sample of three clusters at $0.83 \leq z \leq 1.27$. We exclude from the calculation the cluster MS2053.7−0449, which is at an intermediate redshift ($z = 0.58$), and whose data are relatively shallow. The existence of the candidate cluster CL1645+46 at $z > 1$ was postulated by Jones et al. (1997), following the detection in this direction of a Sunyaev–Zeldovich decrement, as well as a $z = 3.8$, 198–arcsec separation quasar pair, PC1643+4631A&B, which was suggested to be the lensed images of a single source. However, Kneissl, Sunyaev, & White (1998) argue that this cluster must be at $z > 2.8$, based on an improved upper limit on the X-ray emission. Since the observations in our sample cannot detect SNe at such high redshifts, this field is automatically excluded from our calculations of cluster SN rates.

The area of each cluster covered by the observations varies within our sample, with only the cluster core typically covered for the low$-z$ clusters, but also some of the cluster outskirts for the high$-z$ clusters. We therefore limit our calculations of the SN rates to a metric radius of $500h_{50}^{-1}$ kpc around the cluster centres. This region is small enough that significant parts of it are covered by the WFPC2 images available for the low$-z$ clusters, but large enough to include much of the clusters' luminosity. SN 1996cp, which falls slightly outside this arbitrary region, is excluded from the calculations.

Among the SNe we have found within the core regions, two SNe (1999gv and 1996cl) are most probably type-Ia's in their respective clusters, with one occurring in our low-z cluster sample and one in our high-z sample. The high-z sample also includes SN 1996cq, which does not have a host with known redshift, and so may or may not be a cluster SN-Ia. If 1996cq belongs to the $z = 0.83$ cluster in whose field it was found, it is likely a Ia as well, since most core-collapse SNe would be as bright as this event only briefly at this redshift. We will therefore assume we have detected one cluster SN-Ia in the low-z sample, and one or two cluster SNe-Ia in the high-z sample. The 95 per cent confidence ranges on the Poisson expectation values for the number of events in each sample, N, are then $0.07 < N < 4.75$ at low z, and $0.07 < N < 6.3$ at high z, where in the latter case we have taken the union of the 95 per cent probability ranges for observing $i \leq 1$ and $i \geq 2$ events. We propagate these uncertainties into our rate calculations, below.

3.4.2 Rate calculation

The SN rate per stellar luminosity unit in a sample of clusters is obtained by calculating

$$R = \frac{N}{\sum_i \Delta t_i \; f_i \; L_{Bi}}. \tag{2}$$

As detailed below, N is the observed total number of cluster SNe detected, Δt_i is the effective visibility time of a SN-Ia at the cluster redshift, f_i denotes the part of the rest-frame B-band luminosity of a cluster, L_{Bi}, that is probed by our SN search, and the summation is over all observed cluster epochs that are useful for a SN search. By convention, R is often expressed in SNu units, where 1 SNu = 1 SN century$^{-1}(10^{10} L_{B\odot})^{-1}$.

The effective visibility time (sometimes called the "control time") for a given epoch, Δt_i, is the period during which a SN-Ia is above the detection threshold of the data set, weighted by the detection efficiency as a function of magnitude, $\eta(m)$, during this period:

$$\Delta t = \int_{m_{peak,z}}^{m_{lim}} \eta(m) (\frac{dm}{dt})^{-1} dm. \tag{3}$$

Here, $m(t)$ is the SN light curve in the observed band, $m_{peak,z}$ is the maximum-light apparent magnitude of a SN at the redshift of the cluster, and m_{lim} is the limiting magnitude of the observation ($\eta = 0$ for $m > m_{lim}$). SN-Ia light curves in the specific WFPC2 filters and redshifts appropriate to our cluster sample were kindly provided by P. Nugent, based on the data and calculations in Nugent et al. (2001). To allow numerical integration of Eq. 3, $\eta(m)$, which was estimated at discrete values of m in our detection simulations (§3.3.2), was linearly interpolated to a finer grid. The effective visibility times of the sample clusters are listed in Table 5. Note that, due to cosmological time dilation, a given time interval in the observer's frame corresponds to a time shorter by $1 + z$ in the rest frame of a cluster at z. However, each SN light curve is also stretched by $1 + z$, and hence is detectable for a time that is $1 + z$ longer. Due to this cancellation, $1 + z$ time dilation does not figure in N, the total number of SNe detected. The rest-frame SN rate will therefore be proportional to N divided by the rest-frame effective visibility time, as calculated by using, in Eq. 3, SN-Ia light curves without a cosmological $1 + z$ stretch in their time evolution.

As is well documented (e.g., Hamuy et al. 1996; Riess et al. 1998; Perlmutter et al. 1997), SNe-Ia are not a perfectly uniform population, but rather have a non-zero range of peak magnitudes and decline rates, with more luminous SNe fading more slowly and vice versa. Since we are finding of order one or less SNe per cluster, this heterogeneity in the light curves of SNe-Ia introduces an uncertainty in the effective visibility time. For example, in a given cluster, a faint, quickly declining, SN would have a shorter-than-average visibility time, and one needs to account for the probability that such a SN is the one that was detected or missed in that cluster. To this end, we have created a family of SN-Ia light curves with "stretch" factors and correlated peak magnitudes. Based on the distribution observed by Perlmutter et al. (1999), we assume SNe-Ia stretch factors between 0.8 and 1.2, with a corresponding range in peak absolute magnitudes of $-19.5 < M_B < -19.34$. For each of the observed clusters, we then draw a light curve from the distribution and find the effective visibility time. The SN rate for the cluster sample is then calculated. This is repeated many times in a Monte–Carlo process, to gauge the effect of the light-curve non-uniformity on the derived SN rates. We find that the 95 per cent range of the effect on the final rates is about ±7 per cent for the low-z subsample, ±13 per cent for the high-z subsample, and ±10 per cent for the entire sample. Peculiar SNe-Ia (brighter, such as SN 1991T, or fainter, such as SN 1991bg; see, e.g, Li et al. 2001, and references within) are observed to be rare at high$-z$ (Li et al. 2001), and so will have a negligible effect on our derived rates.

The fraction, f_i, of the luminosity probed at a given epoch is calculated by assuming that, within the $500h_{50}^{-1}$ kpc radius we consider, the surface brightness profile has a constant, $50h_{50}^{-1}$ kpc core, and then falls as the projected radius to the -1 power. This is equivalent to assuming the light follows a cored isothermal mass distribution (e.g., Tyson & Fischer 1995). By integrating over the cluster area with useful coverage in the WFPC2 images, we obtain the fraction of the luminosity within $500h_{50}^{-1}$ kpc that was actually searched for SNe. This fraction has a maximum value of $f = 1$ for a cluster in which both available epochs are useful for SN search, and the overlap area includes the entire $500h_{50}^{-1}$-kpc-radius region. Typical values of f_i for our sample are 0.45 for the low$-z$ sub-sample, and 0.75 for the high$-z$ clusters. The values of f_i, multiplied by the useful number of epochs, for each cluster is given in Table 5. Reducing the adopted core radius by a factor of 5 changes the resulting SN rates only by about 5 per cent. Assuming a surface brightness profile that falls (unrealistically) like the square of the radius lowers the SN rate by about 30 per cent.

Normalizing the SN rate to the stellar luminosity requires knowledge of the cluster luminosities in the rest-frame B-band. We have found in the literature luminosities for several of the clusters in our sample. Where necessary, the published values have been corrected to our assumed cosmology. We have taken the V-band luminosities for clusters with $z \sim 0.3$ and the I-band luminosities for clusters with $z \sim 0.85$ as reasonable representations of the rest frame B-band luminosities. Our low$-z$ sample consists of four rich clusters. Abell 2218 and AC114, which have published optical luminosities, are quite similar to Abell 1689 and MS1512.4+3647, which do not (this is also apparent from the *HST* images used in this work), so we have assumed a value of $L_B = 2.5 \pm 0.5 \times 10^{12} h_{50}^{-2} L_{B\odot}$ for the two clusters lacking published data, based on the Abell 2218 and AC114 measurements. Our high$-z$ sample includes two optically rich systems (MS1054.4−0321 and CL1604+4304) shown to be at least as rich as the Coma cluster, with a mean value of $L_B(< 500h_{50}^{-1}\mathrm{kpc}) \sim 5.5 \times 10^{12}\ \mathrm{h}_{50}^{-2}\mathrm{L}_{\mathrm{B}\odot}$. MS1054.4−0321 does not have a published error estimate for its luminosity, and we assume an uncertainty of $\pm 1.5 \times 10^{12}\ h_{50}^{-2} L_{B\odot}$. The third high-$z$ cluster, RXJ0848.6+4453 at $z = 1.27$, presents a difficulty, as it is possibly poorer than the other two. However, few examples of clusters at such high z exist, and estimates of typical luminosities have not been made. We therefore adopt a plausible luminosity value for this cluster of half the mean luminosity of the other two, with a 1σ uncertainty of one half the adopted value. This gives a probable range for the luminosity between zero (equivalent to dropping the cluster from the sample) and the high luminosity of the other two clusters.

To assess the effect of the uncertainties of the cluster luminosities on the rate calculation, we have included in the Monte–Carlo simulation described above, in addition to a light-curve draw, a luminosity draw for each cluster. Each cluster's luminosity was drawn from a Gaussian distribution with mean and σ as given in Table 6. If the uncertainty in the visibility times is not included in the simulation (i.e., only a standard SN-Ia light curve is assumed) the effect of the luminosity uncertainty on the final rates is ±15 per cent at low z, +55 per cent, −30 per cent at high z, and +38 per cent, −20 per cent for the entire sample (95 per cent confidence ranges). The large uncertainty in the luminosity of RXJ0848.6+445 has a minor effect because, at its high redshift, the visibility time of SNe-Ia is short, giving it low weight in the calculation. The uncertainties in the luminosities of the clusters clearly dominate over the uncertainties in the SN-Ia light-curve shape in the final SN-rate errors.

With this input, we obtain from Eq. 2 a rest-frame cluster SN-Ia rate of $R = 0.20^{+0.84}_{-0.19} h_{50}^2$ SNu at $0.18 < z < 0.37$ and $R = 0.41^{+1.23}_{-0.39} h_{50}^2$ SNu at $0.83 < z < 1.27$, where the errors include the 95 per cent confidence Poisson upper and lower limits, as well as the 68 per cent ranges due to the combined light-curve and luminosity uncertainties discussed above. Although the errors are large, we see no indication for any extreme evolution of the SN-Ia rate between the two redshift bins. We therefore also calculate a SN-Ia rate based on the two or three SNe in the combined cluster sample, with $0.18 < z < 1.27$, and a mean redshift (weighted by the rest-frame effective visibility time of each cluster) of $\bar{z} = 0.41$. We find $R = 0.30^{+0.58}_{-0.28} h_{50}^2$ SNu, with the errors having the same meaning as above.

3.4.3 Comparison to models and to other measurements

Table 7 summarises our rate measurements and compares them to those available in the literature. In local elliptical galaxies (which are the dominant population in the central regions of rich clusters), Cappellaro et al. (1997) find $R = 0.067 \pm 0.03 h_{50}^2$ SNu. Among distant field galaxies, measured rates are $R = 0.20^{+0.14}_{-0.09} h_{50}^2$ SNu at $\bar{z} = 0.38$ (Pain et al. 1997) and $R = 0.16^{+0.03}_{-0.02} h_{50}^2$ SNu at $\bar{z} = 0.55$ (Pain et al. 2002; see Fabbro et al. 2000), where the quoted errors are 1σ. The SN-Ia rates we have measured in the central regions of rich clusters at $0.18 < z < 1.27$ are not markedly different from the rates in the local elliptical population, or in the general field population at similar redshifts.

Table 6. Cluster Luminosities and SN-Ia Visibility Times

Cluster	L_B^a [$10^{12}h_{50}^{-2}L_{B\odot}$]	$f_i\times$ No. epochs^b	Δt_i^c [rest-frame days]
Abell 2218	2.5 ± 0.5 ^{d}	1.00	219
Abell 1689	2.5 ± 0.5 ^{h}	0.80	200
AC114	2.5 ± 0.25 ^{e}	0.99	208
MS1512.4+3647	2.5 ± 0.5 ^{h}	0.94	147
MS1054.4−0321	5.5 ± 1.5 ^{f}	1.75	101
CL1604+4304	6.5 ± 2 ^{g}	1.00	105
RXJ0848.6+4453	3 ± 1.5 ^{h}	1.50	19

Notes:
[a] Rest-frame B-band luminosity within $R < 500h_{50}^{-1}$ kpc, and adopted 1σ error, assuming $\Omega_m = 0.3$, $\Omega_\Lambda = 0.7$.
[b] Fraction f_i of the luminosity surveyed for SNe, times the number of epochs used for search.
[c] Effective visibility time, in days, of SNe-Ia at the cluster redshift, in cluster rest-frame.
[d] Squires et al. 1996
[e] Natarajan et al. 1998
[f] Hoekstra, Franx & Kuijken 2000
[g] Postman, Lubin, & Oke 2001
[h] No measurement available in the literature, see text.

Table 7. SN-Ia Rates

Environment	Redshift	SN Rate^a h_{50}^2[SNu]	Reference
Cluster (low−z)	0.25	$0.20^{+0.30}_{-0.13}$	This work
Cluster (high−z)	0.90	$0.41^{+0.47}_{-0.21}$	
Cluster (all)	0.41	$0.30^{+0.21}_{-0.11}$	
E-S0	local	0.07 ± 0.03	Cappellaro et al. (1997)
S0a-Sb	local	0.09 ± 0.03	
Sbc-Sd	local	0.11 ± 0.04	”
Cluster	0.06	$0.11^{+0.06}_{-0.07}$	Reiss (2000)
Field	0.11	$0.10^{+0.07}_{-0.07}$	”
Field	0.10	$0.11^{+0.09}_{-0.05}$	Hardin et al. 2000
Field	0.38	$0.20^{+0.14}_{-0.09}$	Pain et al. 1997
Field	0.55	$0.16^{+0.03}_{-0.02}$	Fabbro et al. 2000

Note: [a] All quoted errors are 1σ.

As mentioned in §1, a major motivation for measuring cluster SN rates is the possibility of addressing directly the puzzle of the large mass of iron and the excess entropy observed in clusters. For example, using gas-dynamical models for ICM enrichment by SNe, Brighenti & Mathews (1998) find that the cluster SN-Ia rate must be $> 1.2h_{50}^2$ SNu today and $> 2.4h_{50}^2$ SNu at $z = 1$ to explain production of most of the iron in the ICM with SNe-Ia. These values are above our 95 per cent upper limits on the cluster SN-Ia rates. We note, however, that the uncertainty in our measured rates is dominated by the large Poisson errors resulting from small number statistics. Even a slightly larger cluster SN sample could more critically test the validity of the SN-Ia ICM enrichment scenario.

4 CONCLUSIONS

We have conducted a search for SNe using data from deep observations of galaxy clusters from the *HST* archive, and have detected six point-like transient events. Based on their observed characteristics and the known properties of different classes of variable objects, we have argued that most or all of these events are SNe. The redshifts and types of the likely host galaxies are available in the literature for five events, demonstrating the benefits of observing well-studied fields.

Folding in the observational parameters of our search, we have compared the numbers and magnitudes of the likely non-cluster (i.e., background or foreground) SNe we have found to published predictions of SN number counts. Such predictions depend strongly on a number of poorly known ingredients, and in particular the luminosity function and extinction of core-collapse SNe. The observed counts from our survey provide some initial constraints on these models. The observed counts, which are comparable to the predictions of DF, but somewhat lower than those of S2000, suggest that at $z \sim 0.7$, core-collapse SNe are relatively faint, due to either extinction or to a luminosity distribution without a high-luminosity tail. However, being based on small SN numbers, these results should be treated with caution, and larger surveys, yielding significantly more events, are definitely called for.

We have used the candidate type-Ia SNe in the clusters to estimate the SN-Ia rate in the central $500h_{50}^{-1}$ kpc of medium-redshift ($0.18 \le z \le 0.37$) and high-redshift ($0.83 \le z \le 1.27$) cluster sub-samples. The measured rates are consistent with SN-Ia measurements in field environments, both locally and at high redshift. Our results argue against an environmental dependence of the SN-Ia rate. Specifically, the observed low SN rate is in conflict with a scenario where SNe-Ia are the primary source of the large amounts of iron seen in the ICMs of massive clusters.

This work shows that useful limits on high−z SN rates and counts can be derived from repeated, deep *HST* imaging, even without any follow-up observations. The current dominant source of uncertainty is the Poisson error due to small number statistics. Next in importance are the lack of identification for some of the SNe, and the uncertainties in cluster luminosities. Obviously, similar analysis of a larger data set would yield SN rates and counts with higher precision, and planned observations (rather than an archival search) would enable some followup work that would reduce the systematic errors. Such an expanded program would also improve the prospects of discovering and utilising gravitationally lensed SNe, as outlined in §1.

Excluding the search for SNe in the HDF by Gilliland et al. (1999), our search is the deepest SN survey conducted, and covers about 6 times the effective area of the HDF search. We find, on average, roughly one SN per deep ($I_{814} > 26$ mag) duplicate WFPC2 cluster field, with about half of the SNe in the clusters and half in the field. At these magnitudes, there is a high density of SNe on the sky, detectable in significant numbers even in the small field of view of the *HST* cameras. Finding these SNe and characterising them, even if only in an incomplete and statistical way, can provide input and constraints to many current issues in astronomy and cosmology. If you are about to carry out deep imaging, whether from space or from the ground, do not do it all at once! Numerous SNe are out there, and can be found simply by splitting the observations into two or more well-separated epochs.

ACKNOWLEDGMENTS

We thank P. Nugent for kindly calculating and providing SN light-curve templates before publication, and helping to resolve the discrepancies in published SN count predictions. We also thank B. Milvang-Jensen and A. Aragón-Salamanca for kindly providing redshifts for galaxies in MS1054.4-0321 prior to publication. N. Brosch, T. Dahlén, P. van-Dokkum, P. Madau, E. Ofek, I. Smail, M. Sullivan, and S. Zucker are thanked for valuable data and advice, and the anonymous referee for numerous useful suggestions. This research has made use of the NASA/IPAC Extragalactic Database (NED), which is operated by the Jet Propulsion Laboratory, California Institute of Technology, under contract with the National Aeronautics and Space Administration. This work was supported by the Israel Science Foundation – the Jack Adler Foundation for Space Research, grant 63/01-1.

REFERENCES

Brighenti, F., & Mathews, W. G. 1998, ApJ, 515, 542

Brighenti, F., & Mathews, W. G. 2001, ApJ, 553, 103

Campusano, L.E., et al., 2001, A&A, submitted, astro-ph/0104477

Cappellaro, E., et al. 1997, A&A, 322, 431

Crawford, C.S., et al. 2001, MNRAS, submitted, astro-ph/0106139

Dahlén, T., & Fransson, C. 1999, A&A, 350, 349 (DF)

Dalal, N., Griest, K., & Pruet, J. 2001, ApJ, submitted, astro-ph/0103436

Della Valle, M. 1991, A&A, 252, L9

Eastman, R.G., Woosley, S.E, Weaver, T.A., & Pinto, P.A. 1994, ApJ, 430, 300

Fabbro, S., et al. 2000, Presentation at the 2000 Moriond meeting "Energy Densities in the Universe", http://moriond.in2p3.fr/J00/mardi/Fabbro

Frail, D., et al. 2001, Nature, submitted, astro-ph/0102282

Frye, B., & Broadhurst, T. 1998, ApJ, 499, L115

Fruchter, A., & Hook, R.N. 1997, Proc. SPIE, 3164, 120

Gal-Yam, A., & Maoz, D. 1999, in "Cosmic Explosions", eds. S. Holt & W. W. Zhang, AIP Conference Proceedings 522, p. 107

Gal-Yam, A., & Maoz, D. 2000, IAU Circ. 7405

Gal-Yam, A., Sharon, K., & Maoz, D. 2001, IAU Circ. 7700, 7701

Gal-Yam, A., & Maoz, D. 2001, in preparation

Gilliland, R.L., Nugent, P., & Phillips, M.M. 1999, ApJ, 521, 30

Hamuy, M., et al. 1996, AJ, 112, 2398

Hoekstra, H., Franx, M., & Kuijken, K. 2000, ApJ, 532, 88

Jones, M. E., et al. 1997, ApJL, 479, L1

Jorgensen, H. E., et al. 1997, ApJ, 486, 110

Kneissl, R., Sunyaev, R.A., & White, S.D.M. 1998, MNRAS, 297, L29

Kolatt, T., & Bartelmann, M. 1998, MNRAS, 296, 763

Kovner, I., & Paczynski, B., 1988, ApJ, 335, L9

Le Borgne, J. F., Pello, R., & Sanahuja, B. 1992, A&AS, 95, 87

Lemonon, L., et al. 1998, A&A, 334, L21

Li, W., et al. 2001, ApJ, 546, 734

Lloyd-Davies, E. J., Ponman, T. J., & Cannon, D. B. 2000, MNRAS, 315, 689

Loewenstein, M. 2000, ApJ, 532, 17

Lubin, L. M., et al. 1998, AJ, 116, 584

Madau, P., Della Valle, M., & Panagia, N. 1998, MNRAS, 297, L17

Mannucci, F., & Ferrara, A. 1999, MNRAS, 305, L55

Milvang-Jensen B., Aragón-Salamanca A., Hau G. K. T., Jørgensen I., Hjorth J. 2002, in preparation

Natarajan, P., Kneib, J., Smail, I., & Ellis, R. S. 1998, ApJ, 499, 600

Norgaard-Nielsen, H.U., et al. 1989, Nature, 339, 523

Nugent, P., et al. 2001, PASP, submitted

Pain, R., et al. 1996, ApJ 473, 356

Pain, R., et al. 2002, ApJ, submitted

Perlmutter, S., et al. 1996, IAU Circ. 6621

Perlmutter, S., et al. 1997, ApJ, 483, 565

Perlmutter, S., et al. 1999, ApJ, 517 ,565

Pettini, M., et al. 2000, ApJ, 528 ,96

Porciani, C., & Madau, P., 2000, ApJ, 532, 679

Postman, M., Lubin, L.M., & Oke, J.B., 2001, AJ, in press, astro-ph/0105454

Reiss, D., Germany, L.M., Schmidt, B.P., & Stubbs, C.W. 1998, AJ, 115, 26

Reiss, D. 2000, PhD thesis, U. of Washington

Riess, A.G., et al. 1998, AJ, 116, 1009

Riess, A.G., et al. 2001, ApJ, in press, astro-ph/0104455

Ruiz-Lapuente, P., & Canal, R. 1998, ApJ, 497, L57

Sadat, R., Blanchard, A., Guiderdoni, B., & Silk, J. 1998, A&A, 331, L69

Sarajedini, V.L., Gilliland, R.L., & Phillips, M.M. 2000, AJ, 120, 2825

Schmidt, B.P., et al. 1998, ApJ, 507, 46

Smail, I., Ivison, R.J., Blain, A.W., & Kneib, J.-P., 1998, ApJ, 507, L21

Squires, G., et al., 1996, ApJ, 461, 572

Sullivan, M., et al. 2000, MNRAS, 319, 549 (S2000)

Tozzi, P., & Norman, C. 2001, ApJ, 546, 63

Trujillo, C.A, Jewitt, D.C., & Luu, J.X. 2001, AJ, 122, 457

Tyson, J.A, & Fischer, P. 1995, ApJ, 446, L55

Tyson, J.A, Kochanski, G.P., & dell'Antonio, I.P. 1998, ApJ, 498, L107

van Dokkum, P. G., et al. 2000, ApJ, 541, 95

Warner, B. 1995, "Cataclysmic Variable Stars", Cambridge University Press

Yungelson, L., & Livio, M. 2000, ApJ, 528, 108